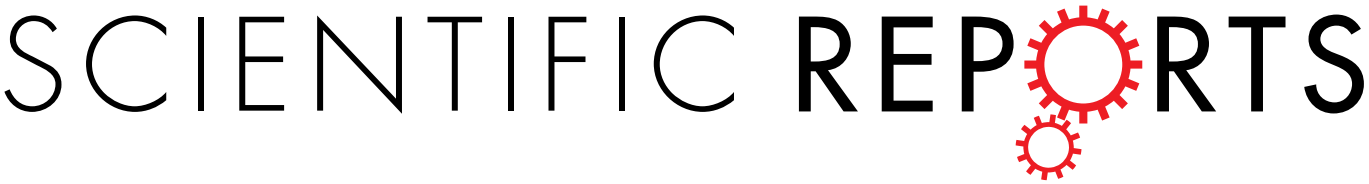

OPEN

Optical Controlled Terahertz Modulator Based on Tungsten Disulfide Nanosheet

Received: 29 June 2017
Accepted: 2 October 2017
Published online: 01 November 2017

Zhiyuan Fan[1,5], Zhaoxin Geng[2], Xiaoqin Lv[1,5], Yue Su[1,5], Yuping Yang[3], Jian Liu[4,5] & Hongda Chen[1]

The terahertz (THz) modulator, which will be applied in next-generation wireless communication, is a key device in a THz communication system. Current THz modulators based on traditional semiconductors and metamaterials have limited modulation depth or modulation range. Therefore, a THz modulator based on annealed tungsten disulfide (WS_2, p-type) and high-resistivity silicon (n-type) is demonstrated. Pumped by a laser, the modulator presents a laser power-dependent modulation effect. Ranging from 0.25 to 2 THz, the modulation depth reaches 99% when the pumping laser is 2.59 W/cm^2. The modulator works because the p-n heterojunction can separate and limit carriers to change the conductivity of the device, which results in a modulation of the THz wave. The wide band gap of WS_2 can promote the separation and limitation of carriers to obtain a larger modulation depth, which provides a new direction for choosing new materials and new structures to fabricate a better THz modulator.

In past decades, the requirements for higher speed and broader bandwidth communication systems have continuously increased. Recently, the terahertz (THz) wave, with a wavelength of 0.03–3 mm, has attracted researchers' attention due to its various advantages in wireless communication. Basic devices for THz wireless communication, such as THz wave sources, THz wave detectors and THz wave modulators, have been investigated by many research groups. Different mechanisms and devices for THz modulators have also been reported[1–5]. THz modulators are based on traditional materials, such as silicon and gallium arsenide (GaAs), and they always have a small modulation depth because of the recombination of carriers in materials[2]. To overcome the small modulation depth, human-made metal micro-nanostructured materials, namely, metamaterials, have been used for THz modulation because metamaterials have many unique optical and electrical properties. For example, in 2006, Chen *et al.* first fabricated a THz modulator based on a metamaterial, which enabled the modulation of THz transmission by 50%[6]. Since then, many studies using THz modulators based on metamaterials have been published[7–9]. These devices provide tuneable, nonlinear and high modulation effects. However, these THz modulators usually work in a specific frequency range that depends on the nanostructure of metamaterials. To achieve both large modulation depth and a wide working range, researchers have sought new materials and structures for THz modulators.

Recently, with the devolvement of two-dimensional (2D) materials, such as graphene and transition metal dichalcogenides (TMDs), some researchers have begun to combine 2D materials with metamaterials to fabricate THz modulators. Ju *et al.* used graphene micro-ribbon arrays to absorb THz waves through plasmon resonance[10]. Graphene metamaterial demonstrated a strong plasmon couple to THz radiation, absorbing over 13% at the plasmon resonance. Because of the complexity in fabricating metamaterials, depositing or transferring 2D materials directly onto a substrate has become another way to fabricate THz modulators. Weis *et al.* first formed a THz modulator based on graphene pumping by a femtosecond laser pulse source[11]. However, it is not practical to use femtosecond lasers in THz communication for commercial applications. Li *et al.* reported a dual control method

[1]State Key Laboratory of Integrated Optoelectronics, Institute of Semiconductors, Chinese Academy of Sciences, Beijing, 10083, China. [2]School of Information Engineering, Minzu University of China, Beijing, China. [3]College of Science, Minzu University of China, Beijing, 100081, China. [4]State Key Laboratory of Superlattices and Microstructures, Institute of Semiconductors, Chinese Academy of Sciences, Beijing, 10083, China. [5]College of Materials Science and Opto-Electronic Technology, University of Chinese Academy of Science, Beijing, 100049, China. Correspondence and requests for materials should be addressed to Z.G. (email: gengsir@163.com) or J.L. (email: liujian@semi.ac.cn)

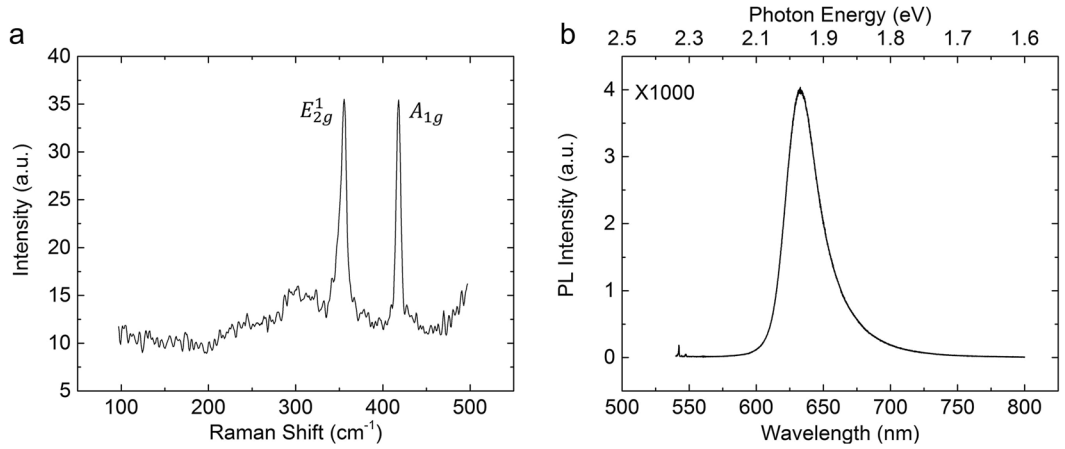

Figure 1. Characteristics of WS_2. (**a**) Raman and (**b**) photoluminescence spectra of WS_2 on a high-resistivity silicon substrate.

for THz modulation based on a graphene-silicon hybrid diode[12]. Continuous wave (CW) source and bias voltage were applied to control the electron transfer between graphene and silicon. Chen *et al.* used another 2D material, molybdenum disulfide (MoS_2), to build an ultrasensitive THz modulator under pumping by a CW source[13]. Unlike graphene, Mo_2 does not have ultrahigh electronic mobility. The working principle of Mo_2-based modulators lies in the band structure of MoS_2. To improve the modulation ability of 2D materials, Cao *et al.* formed an optically tuned THz modulator based on annealed multilayer MoS_2[14]. After an annealing treatment, the MoS_2 was p-type doped, which effectively enhanced the modulation depth. These studies indicated that 2D materials are promising materials for the THz regime and for THz modulators.

Tungsten disulfide (WS_2), as another member of the TMDs, has a similar structure and properties to MoS_2. Each WS_2 monolayer contains a single layer of tungsten atoms sandwiched by two sheets of sulfur atoms in a trigonal prismatic coordination. Like other TMDs, WS_2 exhibits a layer number-dependent band gap. Monolayer WS_2 has a direct band gap of ~2 eV, while multilayer WS_2 and bulk WS_2 have an indirect band gap range from ~1.8 to ~1.3 eV[15]. However, WS_2 has some distinct advantages over MoS_2 and other 2D materials. WS_2 has superior thermal and oxidative stability compared to MoS_2[16,17]. Furthermore, it only has a weak impurity band, which brings it much higher on/off ratios and much larger current in transistors and optoelectronic devices[18,19]. These excellent properties indicate that WS_2 could be used as a new material to fabricate various electronic and optoelectronic devices. Therefore, in this paper, WS_2 was ¬first applied in a THz modulator. The results of the experiment demonstrate that the THz modulator based on annealed WS_2 and silicon has a rather large modulation depth when pumping by a CW source. Compared with reported results of a THz modulator based on MoS_2 and graphene, the WS_2-based device presents a competitive modulation efficiency under similar conditions. Importantly, the working mechanisms of the WS_2- and MoS_2-based modulators are discussed in detail. Based on our analytical model and experiment results, a clear direction for designing more effective THz modulators is noted.

Results and Discussion

Preparation of the THz modulator based on WS2/Si heterostructure. THz modulators work by changing the conductivity of a device, which is primarily determined by the concentration of free carriers in the device. To achieve a significant change in the concentration of free carriers before and after illumination by a laser, lightly doped silicon and materials with long carrier lives, such as germanium, were used in previous work[14,20]. Hence, the substrate in this work was lightly n-type doped, 1-mm-thick high-resistivity (HR, resistivity $\rho > 5000\Omega\cdot$cm) silicon. WS_2 was grown on a sapphire substrate by chemical vapor deposition (CVD). It was later transferred to the substrate with the PMMA-transfer method. The area of WS_2 grown on the substrate was 1 cm × 1 cm. To identify whether the WS_2 thin film existed on the substrate, Raman spectroscopy and photoluminescence were used after transfer. The Raman spectrum, after excitation by a 488-nm laser, is shown in Fig. 1a. Two primary peaks, whose positions were located at 355.5 and 418 cm^{-1}, agree with the results of several reports[21–23]. In addition, we measured the photoluminescence (PL) spectrum of WS_2 to acquire more information about the sample. The results of the PL spectrum indicated that the WS_2 had a band gap of 2.0 eV (Fig. 1b). The results from the Raman and PL spectra indicated that the WS_2 thin film was successfully transferred to the substrate[21,24].

Characterization of the THz modulator based on WS_2/Si heterostructure. The schematic of the final device and measurements are shown in Fig. 2a. All experiments were conducted on a THz time-domain spectroscopy (THz-TDS) system (Fig. 2b). The diameter of the THz beam is approximately 8 mm. The CW laser emits an 808-nm light beam, and the area of the light beam is approximately 1.76 cm^2. During the experiment, a mask was used to limit the laser to illuminating WS_2 only. Considering the impact of the water, which could strongly absorb the THz wave, a closed chamber filled with nitrogen gas was used to cover all the measurement equipment.

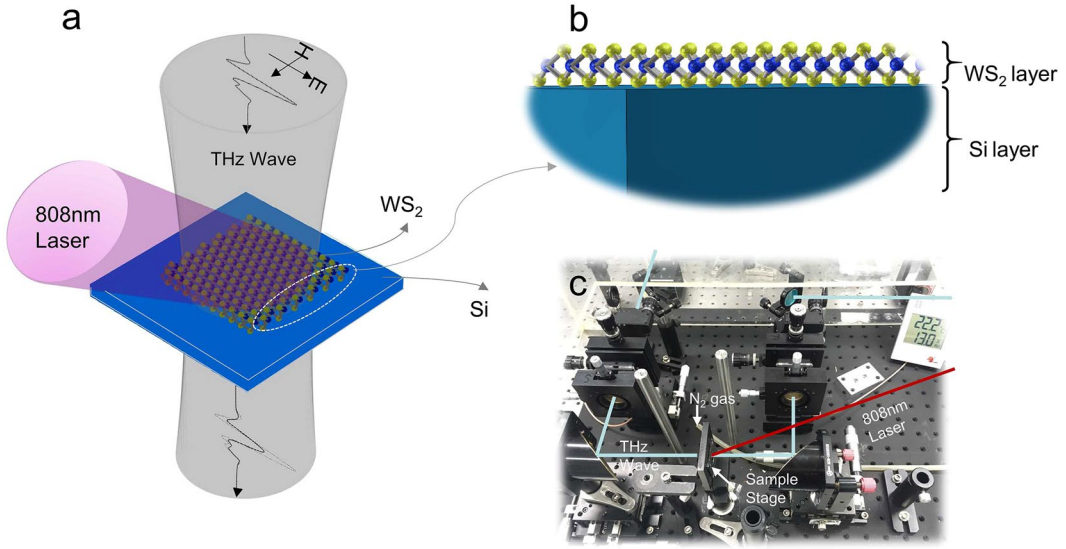

Figure 2. Structure of modulator and testing setup. (**a**) Structure of the THz modulator based on WS_2 and silicon. (**b**) Layer structure of the THz modulator based on WS_2 and silicon (**c**) photoluminescence spectra of WS_2 on a high-resistivity silicon substrate.

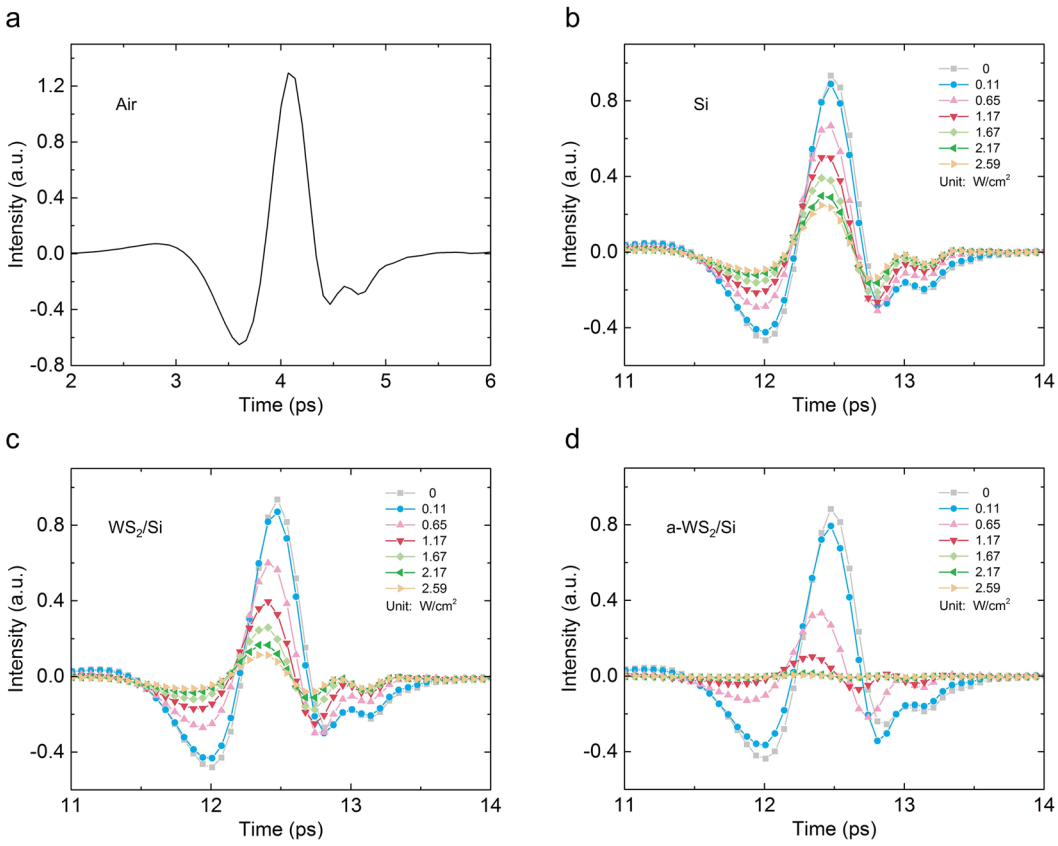

Figure 3. Time-domain intensity of the transmission of the THz signal with different sample under different optical pump power densities. (**a**) Result of the air, (**b**) Result of the HR silicon sample, (**c**) Result of the WS_2/Si sample and (**d**) Result of the a-WS_2/Si sample.

The time-domain spectrum of the THz wave was directly measured by the THz-TDS (Fig. 3). The spectrum of air (Fig. 3a) was measured as a reference to account for the influence of environment factors, such as humidity. The spectrum of HR silicon under different pumping laser power densities was measured at the same time as

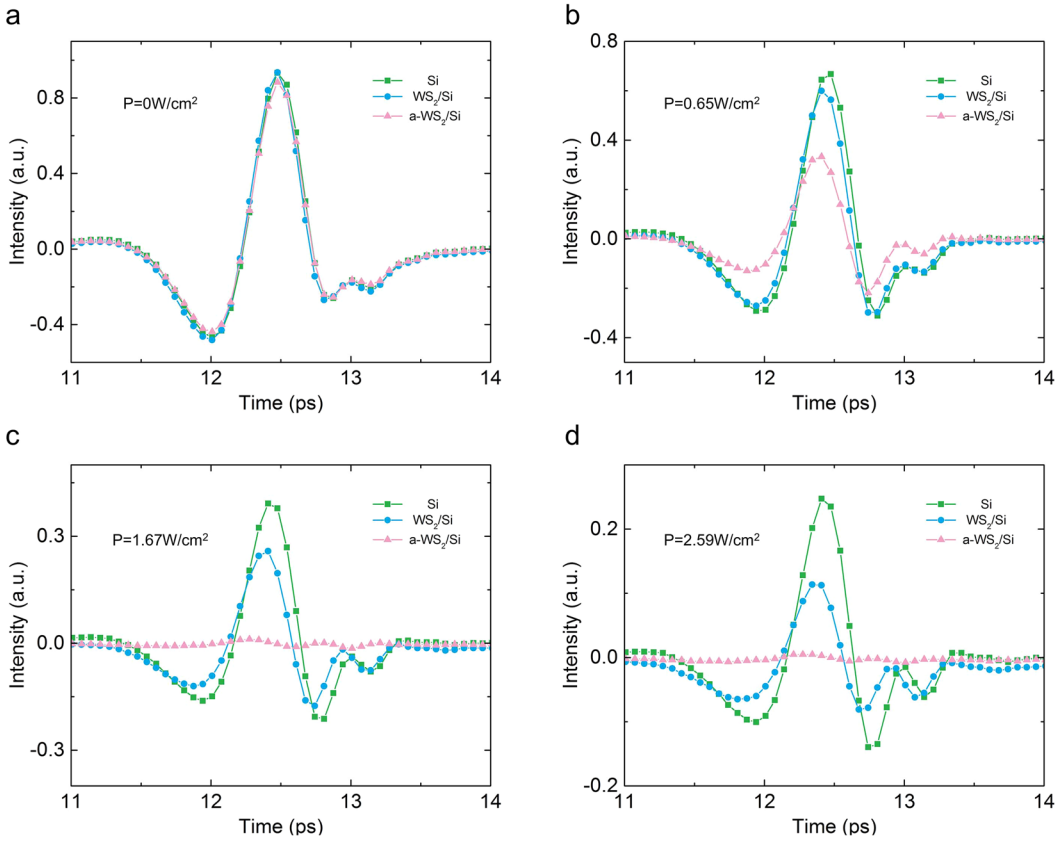

Figure 4. The intensity of transmission of the THz signal by HR silicon, WS_2/Si and a-WS_2/Si samples under same optical pump power densities. The power density of the pumping laser was (**a**) 0 W/cm^2, (**b**) 0.65 W/cm^2, (**c**) 1.67 W/cm^2 and (**d**) 2.59 W/cm^2.

another reference (Fig. 3b). The spectra of HR silicon had a time delay and a height decrease, compared with the spectrum of air. These differences are because the refractive index of silicon is larger than that of air. On the other hand, the shape of these spectra changed little. These results show that there is little absorption in the silicon, and the change of height is mainly due to light reflection.

Figure 3c demonstrates the time-domain intensity of the transmitted THz signal of the WS_2/Si sample under the same conditions as the measurement on HR silicon. With the increased illumination of the pumping laser on the HR silicon and the WS_2/Si sample, the transmission intensity of the THz signal gradually decreased. This indicated that the pumping laser could generate electrons in both the HR silicon and the WS_2/Si samples and these electrons could reflect more THz waves. The intensity of the transmission of the THz signal of the WS_2/Si sample was clearly smaller than that of the HR silicon, which means the interaction between WS_2 and silicon can also influence THz transmission.

The MoS_2 sample can be effectively doped with oxygen and provide numerous holes by annealing in air at the proper temperature[25]. Therefore, WS_2 received the same treatment, because WS_2 has a very similar structure to MoS_2. Hence, the WS_2/Si sample was annealed in air at 300 °C for 5 hours. The WS_2/Si sample, after annealing (a-WS_2/Si sample), was also measured on the THz-TDS system. The time-domain intensity of the transmitted THz signal of the a-WS_2/Si sample is shown in Fig. 3d. The intensity of the THz signal was significantly reduced after transmitting the a-WS_2/Si sample, compared with the transmission spectra of the HR silicon and the WS_2/Si samples. These results illustrate that the annealing treatment could effectively reduce the THz transmission of the sample.

For a clearer observation of the modulation effect for a different sample, the time-domain intensity of the transmission of the THz signal under the same pumping laser power is demonstrated in Fig. 4. Without illumination by the pumping laser, the intensity of the transmission of the THz signal had few differences between the HR silicon, WS_2/Si and a-WS_2/Si samples (Fig. 4a), which meant that WS_2 is almost transparent for the THz wave.

When the power density of the laser was increased to 0.65 W/cm^2, the WS_2 and the a-WS_2/Si samples demonstrated a lower intensity of transmission for the THz signal than that of the HR silicon (Fig. 4b).

When the power density of the laser increased to 1.67 and 2.59 W/cm^2, the difference in the transmission for the THz signal between the HR silicon and WS_2/Si increased. In particular, the intensity of the THz signal decreased to almost zero when it was transmitted through the a-WS_2/Si sample at same time (Fig. 4c,d). The results in Fig. 4 indicate that both the WS_2/Si and a-WS_2/Si samples could reflect more THz waves than the HR silicon sample when illuminated by the laser. Specially, a-WS_2/Si had a lower intensity of transmission for the THz signal under a low pumping power density compared with the results of the WS_2/Si and HR silicon samples.

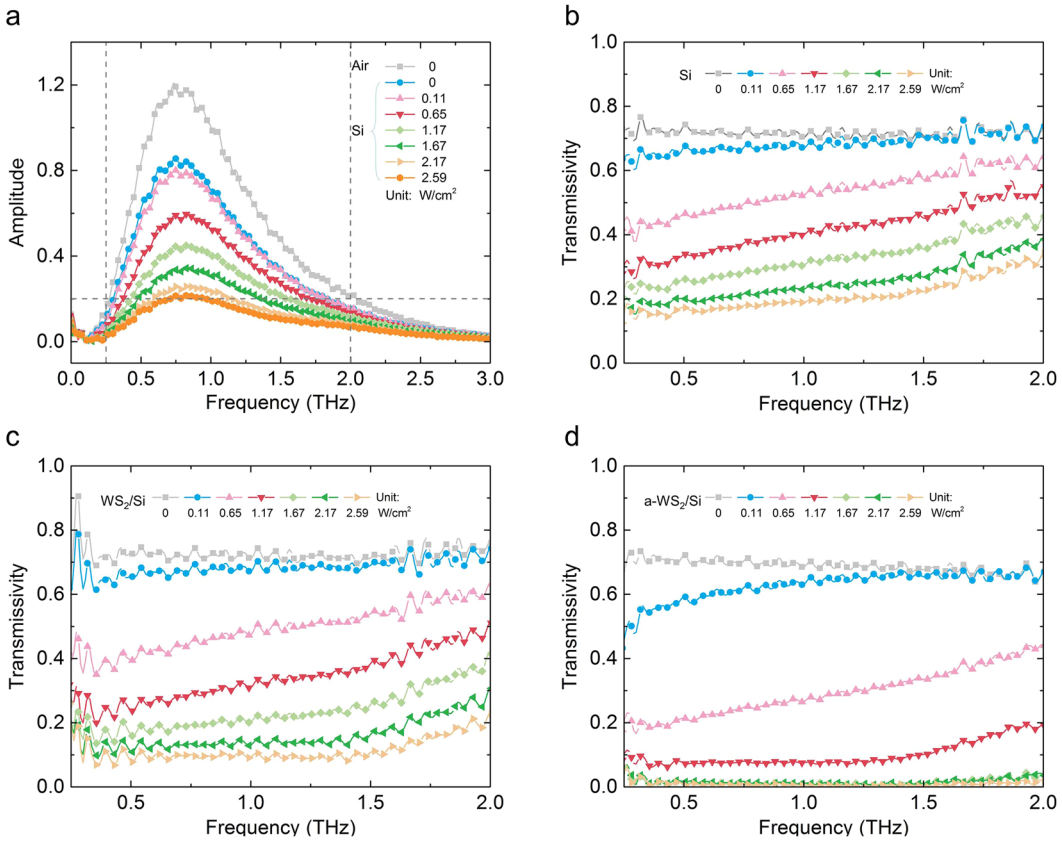

Figure 5. Frequency-domain intensity of THz amplitude and the transmission of the THz signal with different sample under different optical pump power densities. (**a**) Relationship between amplitude and frequency of air and silicon. Relationship between THz transmissivity and frequency of the (**b**) HR silicon, (**c**) WS_2/Si and (**d**) a-WS_2/Si samples.

The fast Fourier transfer (FFT) method was applied to transfer data from the time domain into data in the frequency domain. The amplitude of the THz wave acquired from the results of the FFT method is shown in Fig. 5a. The effective part of frequency domain signal is from 0.25 to 2 THz due to limits of the THz generator and detector. THz transmissivity was calculated by Equation 1:

$$T = \frac{A_s}{A_0} \tag{1}$$

where A_S and A_0 represent the THz wave amplitude after crossing the sample and air, respectively. The relationship between the transmissivity of the samples and the frequency under different pumping laser power densities is shown in Fig. 5b–d. As the power density of the pumping laser increased, the THz transmissivity of all samples decreased. As the frequency increased from 0.25 to 2.0 THz, the transmissivity of the HR silicon sample increased slightly, which indicated that the THz modulator based on HR silicon could not work at high frequencies.

However, for the WS_2/Si and the a-WS_2/Si samples, the increase began at 1.5 THz due to the limit of the Drude model, which has been discussed in ref.[8]. These results illustrate that the WS_2/Si and a-WS_2/Si samples could stably work from 0.25 to 1.5 THz.

The lowest THz transmissivity of a-WS_2/Si sample measured in this work was an average of 0.736%, ranging from 0.25 to 2.0 THz, when the pumping laser power was 2.59 W/cm^2. A relatively low THz transmissivity was reached, 1.385%, when the pumping laser power was 1.67 W/cm^2. The modulation depth was also calculated for a clear comparison with other THz modulators. The computational formula for modulation depth is Equation 2:

$$M = \left| \frac{(T_i - T_0)}{T_0} \right| \tag{2}$$

where T_i and T_0 are the THz transmissivity with and without pumping light, respectively. The modulation depth of the HR silicon, WS_2 and a-WS_2/Si samples is demonstrated in Fig. 6a–c. At different frequencies, the modulation depth of the same sample at the same pumping power density is different. The results (Fig. 6) show that the HR silicon and WS_2/Si samples declined significantly in modulation depth when the frequency increased from 0.5 to 2.0 THz under the same pumping power density. However, the a-WS_2/Si sample had a small decline of modulation depth when the frequency increased. In particular, when the pumping power density was larger than

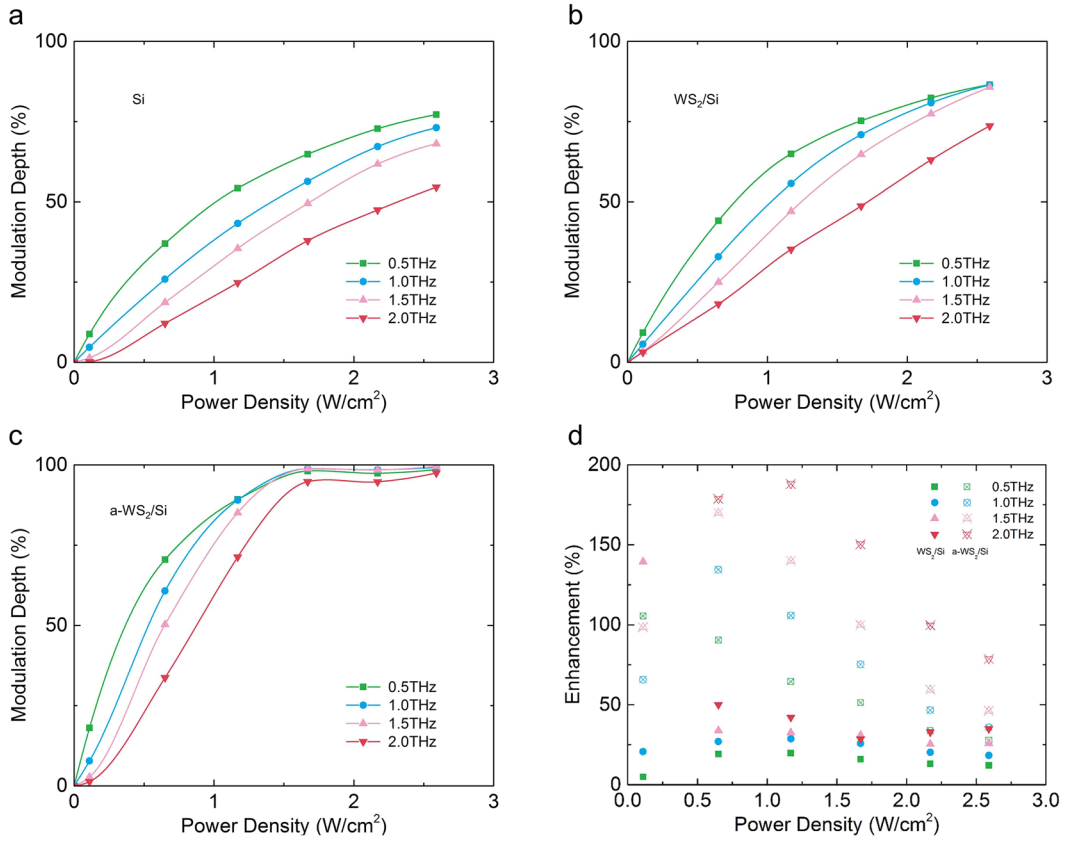

Figure 6. Modulation depth of different samples and the enhancement. (**a**) HR silicon, (**b**) WS_2/Si and (**c**) a-WS_2/Si samples under different pumping power densities and at different frequencies. (**d**) Enhancement rate of the WS_2/Si and the a-WS_2/Si samples compared with the HR silicon sample.

1.67 W/cm^2, the modulation depth of the a-WS_2/Si sample declined little compared with that of the HR silicon and the WS_2/Si samples. In Fig. 6d, we demonstrated the enhancement rates of the WS_2/Si and the a-WS_2/Si samples compared with that of the HR silicon sample.

Removing data caused by noise, Fig. 6d demonstrates that the a-WS_2/Si sample had a 188% enhancement (E) compared with that of the HR silicon sample, which was calculated by Equation 3:

$$E = \left| \frac{(M_S - M_{Si})}{M_{Si}} \right| \tag{3}$$

where M_S represents the modulation depth of the WS_2/Si and a-WS_2/Si samples; and M_{Si} represents the modulation depth of the HR silicon. The calculation was carried out when the data had the same frequency and power density.

Discussion

The conductivity of materials affects the transmission of the THz wave[13,14,26]. Hence, the modulation depth of the THz modulator based on the WS_2-silicon heterojunction is mainly determined by the conductivity of the device, which changes with the behaviour of the carriers. Therefore, analysing and understanding the behaviours of the carriers is the key point in understanding the mechanism by which THz modulators work.

During the experiment, the transmissivity of all samples declined when the pumping laser illuminated samples. This indicated that the conductivity of the devices changed because free carriers were generated in the materials after absorbing photons. Since the laser is 808 nm (1.53 eV), most light transmitted the WS_2 ($E_g = 2$ eV) and was absorbed by silicon ($E_g = 1.12$ eV). As silicon absorbed most of the light, photogenerated carriers were mainly generated in silicon. Without WS_2, these photogenerated carriers could not exist in silicon for very long due to recombination, which limited the number of electrons, as well as changes in the conductivity of the device. An effective way to break this limitation is separating electrons and holes into different areas to prevent collision. The built-in electric field in the WS_2-silicon heterojunction could promote the separation, and this is a key factor in WS_2-silicon-based THz modulators.

In the WS_2-silicon sample that was not annealed, both WS_2 and silicon have Fermi levels near the centre of the bandgap with slight difference (Fig. 7a). Therefore, a I-type heterojunction was formed when they came into contact (Figs. 4e and 7c). Electrons and holes generated in silicon cannot be effectively separated and are easily recombined due to collision. Recombination between the electron and the hole leads to a slight change in the

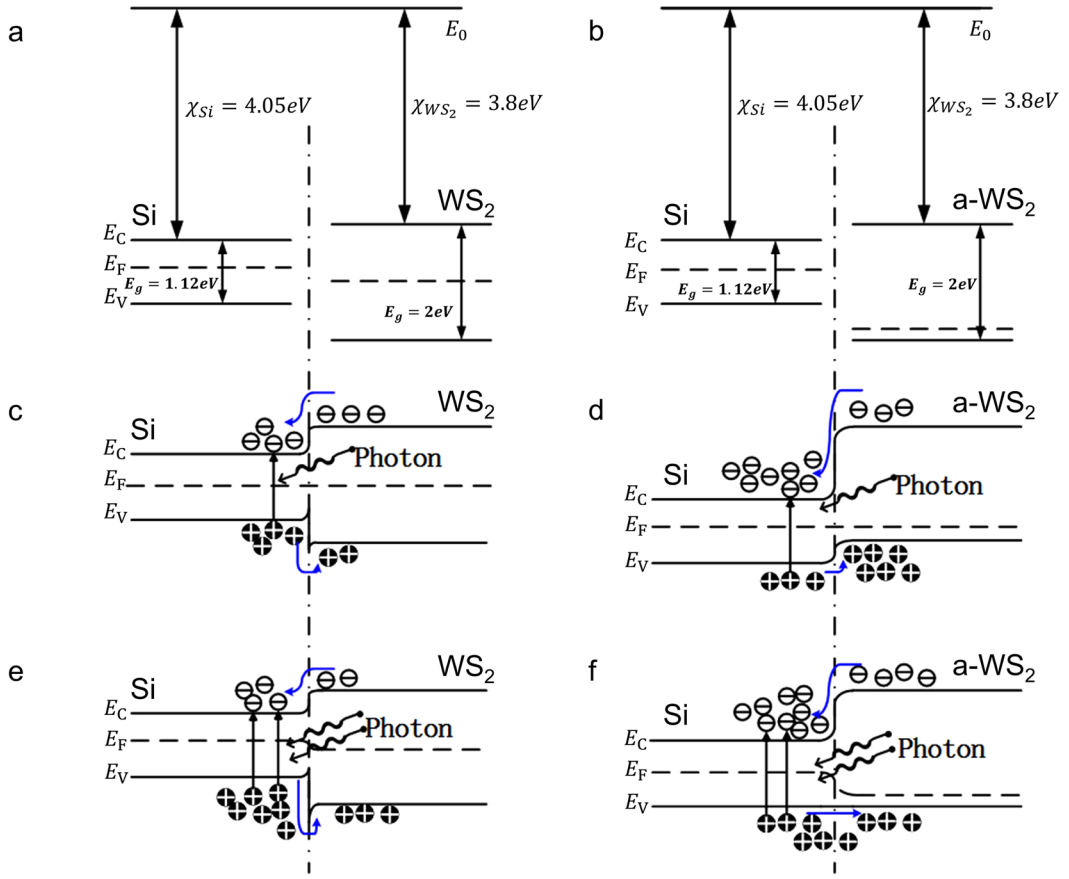

Figure 7. Energy band structure of different samples. (**a**) Energy band structure of the high-resistivity silicon, WS_2 and (**b**) a-WS_2 before contact. Band structure of the WS_2-Si sample before annealing under (**c**) low and (**e**) high pumping laser power. Band structure of the WS_2-Si sample after annealing under (**d**) low and (**f**) high pumping laser power.

concentration of free carriers as well as a slight change in the conductivity of a device. After an annealing treatment, WS_2 became a p-type semiconductor and formed a II-type heterojunction with the HR silicon (Fig. 7b). In the II-type heterojunction, the potential barrier for electron V_D was calculated by Equation 4:

$$V_D = \left|\left(E_0 - E_{F(Si)}\right) - \left(E_0 - E_{F(WS_2)}\right)\right| \tag{4}$$

where the E_0 represents the vacuum electron energy. $E_{F(Si)}$ and $E_{F(WS_2)}$ represent the fermi level in silicon and WS_2 respectively. The annealing treatment lower the fermi level in WS_2 which leading to a larger V_D as well as a larger built-in electric field. Under the electrostatic force of the built-in electric field, photogenerated electrons were transferred from WS_2 to silicon, or in other words, they were limited in silicon (Figs 4f and 7d). On the other hand, holes moved in the opposite direction and combined in WS_2. Therefore, electrons and holes were separated and limited in different areas of the device. The separation in space made it hard for the electrons and holes to meet each other and collide. The low collision probability resulted in the long life time of the free carriers. As more electrons were generated and localized in the silicon, the conductivity of the silicon was enhanced. Based on the theory of electromagnetic fields, the THz wave would be reflected by materials with high conductivity. Therefore, a THz modulator based on a WS_2-silicon heterojunction was demonstrated.

THz modulators based on WS_2/Si and MoS_2/Si have similar structures. Hence, the working mechanism of these modulators is also similar. A key factor of the working mechanism lies in the separation of free carriers, which is promoted by the built-in electric field. However, the results show that the WS_2-silicon sample has a larger modulation depth than the MoS_2-silicon sample. The difference in the band gap between WS_2 and MoS_2 is a key point to explain this result. When two materials come into contact, a potential barrier, which is mainly determined by the band structure of two materials, is formed along with a built-in electric field. The potential barrier can influence the diffusion of carriers, while the built-in electric field mainly influences the drift of carriers. The height of the potential barrier, which is determined by the difference in the conduction band minimum and valance band maximum of the materials, influences whether the carriers can diffuse between the two materials. Unlike carrier drift under the force of the built-in electric field, carriers diffusing from areas of high concentration those with low concentration need to overcome the force of the electric field and potential barriers. The number of electrons in silicon will increase as the power of the laser increases. The force of the electric field will decrease

Year	Materials	Treatment	Modulation Depth	Motivative Laser	Ref
—	WS_2	CVD, PMMA-transfer and annealing	99%	808 nm, 2.59 W/cm^2	This work
2012	Graphene	CVD and thermal release tape transfer	99%	780 nm, 1.6×10^4mW/cm^2	11
2014	C_{60}	Thermal evaporation deposited, annealing	98%	785 nm, 955 mW/cm^2	27
2015	AlClPc	Thermal evaporation deposited	99%	450 nm, 1.57 mW/cm^2	3
2015	Graphene	CVD, PMMA-transfer	83%	532 nm, 420 mW; −4V bias voltage	12
2016	MoS_2	CVD, PMMA-transfer and annealing	96%	808 nm, 4.56 W	14
2016	MoS_2	CVD	75%	532 nm, 0.24 W/cm^2	13

Table 1. Some results of reported THz modulator based on materials-silicon heterostructure.

due to electron accumulation; the potential barrier will also decrease due to changes in the band structure (Fig. 7); and the diffusion rate of electrons will increase due to the larger difference in the electron concentration. For holes, the drifting rate is larger than the diffusion rate because the difference in the concentration of the holes is rather small. These discussions indicated that there was a limitation in the modulation depth that was decided by the balance between the built-in electric field, electron concentration and potential barrier. Both MoS_2 and WS_2 could hardly form the III-type heterojunction with silicon. Therefore, the potential barrier should meet the Formula 5:

$$V_D \ll E_{g(XS_2)} \tag{5}$$

where $E_{g(XS_2)}$ represents the band gap of MoS_2 or WS_2. Since $E_{g(WS_2)}$ is larger than $E_{g(MoS_2)}$, WS_2-silicon heterojunction could achieve a higher potential barrier than MoS_2-silicon heterojunction. The larger potential barrier could effectively prevent electrons from diffusing from silicon to WS_2 which leading to a larger modulation depth when illuminated by a high-power pumping laser.

The Table 1 listed the results of THz modulator based on TMDs, graphene and other material-silicon heterostructure. Comparing to C_{60} and AlClPc (Chloride aluminium phthalocyanine), WS_2 is thinner, more stable and compatibility with silicon process. Comparing to graphene, WS_2 demonstrated competitive modulation depth while needed lower motivation power. Among the TMDs, WS_2 demonstrated larger modulation depth as analysed above.

Methods

WS_2 Transfer. The 1 cm × 1 cm WS_2 thin film was grown on a sapphire substrate using the CVD method. PMMA/anisole solution was dropped on the surface and covered all the WS_2. After the anisole in the solution evaporated, a NaOH solution (~3 mol/L) was used to etch the sapphire substrate. WS_2 and PMMA were separated from the sapphire substrate. The WS_2/PMMA film was transferred to a high-resistivity silicon substrate whose size was 1.5 cm × 1.5 cm. Finally, the PMMA was dissolved by acetone.

Annealing treatment. The WS_2/Si sample was annealed on air. The heating rate was set as 10 °C/min. The annealing temperature was set at 300 °C and the annealing time was 5 hours. After being heated, the sample was cooled naturally.

THz measurement. The sample was measured using a THz time-domain spectroscope system. N_2 gas was used to protect the sample and maintain dry conditions during the measurement. The avenge relative humidity rate during measurements was 9%.

Conclusions

In conclusion, a THz modulator based on a WS_2-Si heterostructure was presented in this work. The modulation effect could be modified by changing the power of pumping laser. After being annealed in air, the THz modulation depth of the modulator was significantly enhanced. The largest modulation depth reached 99%, ranging from 0.25 to 2 THz when the power of pumping laser was 2.59 W/cm^2. An analytical model was proposed to explain the large modulation depth of the THz modulator based on the annealed WS_2-silicon heterojunction. WS_2 became a p-type semiconductor after the annealing treatment and formed a p-n heterojunction with the n-type HR silicon. The p-n heterojunction could separate electrons and holes quickly and effectively. On the other hand, WS_2 has a wide band gap that forms a high potential barrier at the interface, which could prevent electrons from diffusing to WS_2. Therefore, a rather high conductivity of the sample was obtained, which resulted in a larger THz modulation depth. These results indicate that WS_2 is a promising material for THz modulators. Based on our analytical model, 2D materials with wider band gaps, such as boron nitride (BN), and 2D material heterojunctions, which can separate carriers quickly and effectively, might be novel and promising choices for THz modulators.

References

1. Kužel, P. & Kadlec, F. Tunable structures and modulators for THz light. *Comptes Rendus Physique* **9**, 197–214 (2008).
2. Rahm, M., Li, J.-S. & Padilla, W. J. THz Wave Modulators: A Brief Review on Different Modulation Techniques. *Journal of Infrared, Millimeter, and Terahertz Waves* **34**, 1–27 (2013).
3. He, T. *et al*. High-efficiency THz modulator based on phthalocyanine-compound organic films. *Applied Physics Letters* **106**, 053303 (2015).

4. Wilk, R., Vieweg, N., Kopschinski, O. & Koch, M. Liquid crystal based electrically switchable Bragg structure for THz waves. *Opt Express* **17**, 7377–7382 (2009).
5. Ma, Y., Saha, S. C., Bernassau, A. L. & Cumming, D. R. S. Terahertz free space communication based on acoustic optical modulation and heterodyne detection. *Electronics Letters* **47**, 868 (2011).
6. Chen, H.-T. *et al*. Active terahertz metamaterial devices. *Nature* **444**, 597–600 (2006).
7. Chen, H.-T. *et al*. A metamaterial solid-state terahertz phase modulator. *Nature Photonics* **3**, 148–151 (2009).
8. Gu, J. *et al*. Active control of electromagnetically induced transparency analogue in terahertz metamaterials. *Nature Communications* **3**, 1151 (2012).
9. Karl, N. *et al*. An electrically driven terahertz metamaterial diffractive modulator with more than 20 dB of dynamic range. *Applied Physics Letters* **104**, 091115 (2014).
10. Ju, L. *et al*. Graphene plasmonics for tunable terahertz metamaterials. *Nature Nanotechnology* **6**, 630–634 (2011).
11. Weis, P. *et al*. Spectrally Wide-Band Terahertz Wave Modulator Based on Optically Tuned Graphene. *ACS Nano* **6**, 9118–9124 (2012).
12. Li, Q. *et al*. Active graphene–silicon hybrid diode for terahertz waves. *Nature Communications* **6**, 7082 (2015).
13. Chen, S. *et al*. Ultrasensitive terahertz modulation by silicon-grown MoS_2 nanosheets. *Nanoscale* **8**, 4713–4719 (2016).
14. Cao, Y. *et al*. Optically tuned terahertz modulator based on annealed multilayer MoS_2. *Scientific Reports* **6**, 22899 (2016).
15. Zeng, H. *et al*. Optical signature of symmetry variations and spin-valley coupling in atomically thin tungsten dichalcogenides. *Scientific Reports* **3** (2013).
16. Sliney, H. E. Solid lubricant materials for high temperatures—a review. *Tribology International* **15**, 303–315 (1982).
17. Braga, D., Gutiérrez Lezama, I., Berger, H. & Morpurgo, A. F. Quantitative Determination of the Band Gap of WS_2 with Ambipolar Ionic Liquid-Gated Transistors. *Nano Letters* **12**, 5218–5223 (2012).
18. Georgiou, T. *et al*. Vertical field-effect transistor based on graphene–WS_2 heterostructures for flexible and transparent electronics. *Nature Nanotechnology* **8**, 100–103 (2012).
19. Zhao, W. *et al*. Lattice dynamics in mono- and few-layer sheets of WS_2 and WSe_2. *Nanoscale* **5**, 9677 (2013).
20. Wen, Q.-Y. *et al*. Graphene based All-Optical Spatial Terahertz Modulator. *Scientific Reports* **4**, 7409 (2014).
21. Berkdemir, A. *et al*. Identification of individual and few layers of WS_2 using Raman Spectroscopy. *Scientific Reports* **3** (2013).
22. Gaur, A. P. S., Sahoo, S., Scott, J. F. & Katiyar, R. S. Electron–Phonon Interaction and Double-Resonance Raman Studies in Monolayer WS_2. *The Journal of Physical Chemistry C* **119**, 5146–5151 (2015).
23. McCreary, K. M. *et al*. The Effect of Preparation Conditions on Raman and Photoluminescence of Monolayer WS_2. *Scientific Reports* **6** (2016).
24. Gutiérrez, H. R. *et al*. Extraordinary Room-Temperature Photoluminescence in Triangular WS_2 Monolayers. *Nano Letters* **13**, 3447–3454 (2013).
25. Nan, H. *et al*. Strong Photoluminescence Enhancement of MoS_2 through Defect Engineering and Oxygen Bonding. *ACS Nano* **8**, 5738–5745 (2014).
26. Zheng, W., Fan, F., Chen, M., Chen, S. & Chang, S.-J. Optically pumped terahertz wave modulation in MoS_2 -Si heterostructure metasurface. *AIP Advances* **6**, 075105 (2016).
27. Yoo, H. K. *et al*. Highly efficient terahertz wave modulators by photo-excitation of organics/silicon bilayers. *Applied Physics Letters* **105**, 011115 (2014).

Acknowledgements

The project was supported by funds from The National Key Research and Development Plan (2017YFB0405405, 2017YFB0405402, 2016YFB0402702, 2016YFB0402705, 2016YFA0202201, and 2016YFA0202202), The National Natural Science Foundation of China (61774175, 61335010, 61674146, 61378058 and 11574408), The Major State Basic Research Development Program of China (973 Program) (2015CB352100) and the National Instrumentation Program (No. 2012YQ14000508).

Author Contributions

Z. F. fabricated the samples, measured the THz spectra and Raman spectra of the samples, and performed theoretical analysis. Z.G. proposed the WS_2-based modulator, designed the experiments and guided the whole process in the experiments. P.Y. offered help taking measurements. Z.F., J.L., Z.G., X.L., Y.S. and H.C. contributed to the writing and revising of the manuscript. All authors discussed the results.

Additional Information

Competing Interests: The authors declare that they have no competing interests.

Publisher's note: Springer Nature remains neutral with regard to jurisdictional claims in published maps and institutional affiliations.